

Finite Wings

Felicity Cundiff, Angelina dos Remedios, Peter Funston, Kyle Klem AA 321 Aerospace
Laboratory, Section AB

William E. Boeing Department of Aeronautics, University of Washington

November 14, 2023

I. Procedure

This experiment took place in the Kirsten Wind Tunnel (KWT) in the test section shown in Figure 1. There were six main apparatus used throughout this experiment: a NACA 23012 wing, the circular wing end caps, the flow visualization fluid and applicator, a black light, the Kirsten Wind Tunnel balance, and a camera. The data acquisition system (DAQ) was the primary piece of data collection software used throughout the lab. The DAQ used an online plotting PC and a data acquisition PC.

The tests were to be conducted at two different values of indicated pressure, 10 psf and 35 psf. The tests were to be conducted at an angle of attack of -4° through $+10^\circ$ in 2° steps. After $+10^\circ$ was reached, the tests were to reach $+20^\circ$ in 1° steps. Then using the same increments, the data was collected going back to zero. The KWT team operated the wind tunnel for the tests; they calibrated the angle of attack, conducted a strut tare experiment, and mounted the wing before the tests took place. After this, the following steps were taken:

1. Measured the geometric parameters of the wing (i.e. c, b, t_{max}) and noted the positions of the "trip dots"
2. Discussed the tare procedure and the angle of attack calibration procedure and why they were needed with the crew
3. Repeated the following steps for the wing with and without the end caps
 - (a) Measured the loads on the wing for two different values of indicated pressure, 10 psf, and 35 psf, while sweeping through an angle of attack starting at -4° going to $+10^\circ$ in 2° steps
 - (b) After $+10^\circ$ was reached, the loads on the wing were measured through $+20^\circ$ in 1° steps
 - (c) From the load data, the stall angle for the wing at each value of indicated pressure was determined.
 - (d) A surface flow visualization of the surface flow patterns on top of the wing for a chosen angle was conducted by applying visualization fluid and observing the change of the fluid underneath a blacklight at an indicated pressure of 35 psf. The angle at which the surface flow visualization took place was recorded
4. Notes and photos of the tests were taken; the KWT staff provided all pertinent data and digital photos

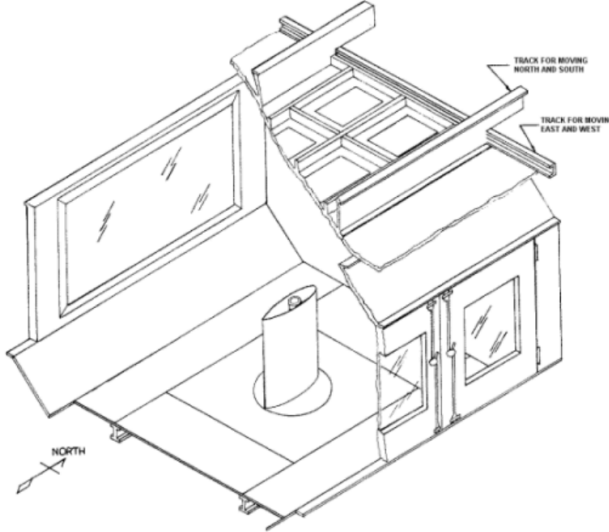


Fig. 1: KWT Cutaway

Data was provided in the form of a .csv file. Data analysis was done in MATLAB. Tares that did not align well with the angles of attack of the test points were interpolated. The resulting data was then subtracted. The effect of fork was used as a tare. Using the force balancing matrix, the lift, drag, and moment were calculated. The drag and moment were then calculated after tare. Graphs were made within MATLAB.

II. Discussion of Results

The main purpose of this investigation is to study the variation of lift, drag, and pitching moments of a finite wing using the Kirsten Wind Tunnel (KWT). The key dimensions of the wing are a reference area of 9.375 ft^2 , a reference span of 90 inches, and a mean aerodynamic chord (MAC) of 15 inches. By analyzing the effects of circular end caps as a function of angle of attack, we aim to gain a better understanding of the impact of viscosity and Reynolds number on the pressure field, lift, and drag of the wing. This includes investigating the effects of wingtip vortices and boundary layer separation on the lift and drag of the wing.

Using matrix 4 as well as the given data for the strut drag, tare data, and the weight tare data, the raw forces can be used to calculate corrected forces and moments. The corrected forces and moments at an angle of attack of 10 degrees is $L_R = 79.6611 \text{ lbs}$, $D_R = 5.1982 \text{ lbs}$, and $M_{P,R} = -5.7678$. Both the corrected lift and drag are close to the corrected lift and drag provided by KWT. Some deviation is expected since the full correction process is more complicated than applying 5 and 6. The corrected moment does seem significantly different as it is about 6.5 lb-ft greater than the corrected moment given by KWT. This seems to suggest either an error in the methodology, or that the corrections done by KWT for the moment are more complex than that of Lift and Drag.

$$C_L = \frac{LR}{qS} \quad (1)$$

$$C_D = \frac{DR}{qS} \quad (2)$$

$$C_M = \frac{MPR}{qSc} \quad (3)$$

$$\begin{bmatrix} L \\ D \\ M_P \end{bmatrix} \begin{bmatrix} a1 & b1 & c1 \\ a2 & b2 & c3 \\ a3 & b3 & c3 \end{bmatrix} = \begin{bmatrix} L_R \\ D_R \\ M_{P,R} \end{bmatrix} \quad (4)$$

$$D_{aftertare} = D_{beforetare} - (NDrag) * q \quad (5)$$

$$M_{P,afterweighttare} = M_{P,beforeweighttare} - (PMWT) \quad (6)$$

Surface flow patterns during a stall is the result of airflow separation from the body being observed, specifically from the upper wing. This causes turbulence, which leads to a decrease in lift and an increase in drag, it can also cause vibrations in the aircraft's wings. The surface flow patterns during wing stall are important to improving the design to better handle stall conditions.

End caps affect the flowfield and forces/moment on the wing. Adjusting the size and shape of the end caps can alter vortex flow patterns, lift, drag, and moment acting on the wing, and increase the effective aspect ratio of the wing. Aspect ratio is equal to $\frac{(Span)^2}{Area}$, plugging in our given values for span and Area we get an aspect ratio of 6.

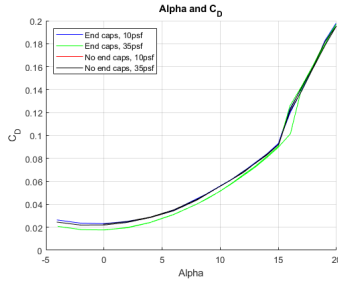


Fig. 2: Plot of coefficient of drag vs. angle of attack.

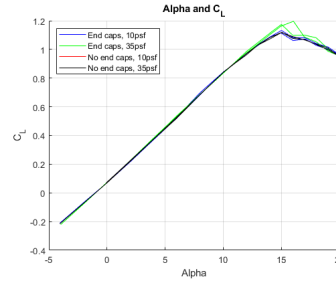


Fig. 3: Plot of coefficient of lift vs. angle of attack.

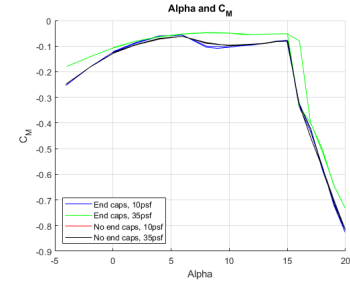


Fig. 4: Plot of coefficient of moment vs. angle of attack.

The span efficiency factor (e) and parasitic drag coefficient ($C_{D,p}$) can be determined using 7. Using data from the test at 10 psf, with end caps on the wing, the values of e and $C_{D,p}$ are 1.15 and 0.0225 respectively. This demonstrates how a finite length of wing causes there to be an increased amount of drag and less lift.

In order to calculate the 3D lift-curve slope from our 2D lift-curve slope we use Equation 8. After inputting the span efficiency (e), the Aspect ratio (AR), and 2D lift-curve slope α_0 the result is a 3D lift-curve slope of 0.731. This is 0.026 less than the 2d lift-curve slope of 0.757. This difference is caused by vortices created at the ends of the wing which cause less lift generated.

$$C_D = C_{D,p} + \frac{1}{(\pi A Re)} C_L^2 \quad (7)$$

$$\frac{dC_L}{d\alpha} = \frac{\alpha_0}{1 + \frac{\alpha_0}{\pi A Re}} \quad (8)$$

Observing flow visualizations is important to build a better understanding of the flow dynamics. In this lab both the wing with end caps and without went through a flow visualization test. Both tests resulted in similar patterns except for one aspect. On the test with no end caps test there was lots of turbulence on the end and with the end cap there was not. This helps to confirm the conclusion that adding end caps will reduce the turbulence caused at the wing tip.

Larger aspect ratios reduce a wings induced drag, however, that's not always the most pressing issue when designing wings for an aircraft. Often times there are restrictions on how wide an air crafts wings can be, this combined with needing enough lift to make sure the craft can fly are just a few reasons as to why higher aspect ratios aren't always used.

Circular end caps were used in this lab as they are a good baseline for the benefits of having end caps on wings. Having a purely circular end cap may not be the best design however, there are probably cases in which doing something as simple as adding circular end caps can help improve efficiency.

During this lab there were some hysteresis produced as the wing pitched down from 20 degrees to 15. This can be best seen in the test at 35 psf with end caps as the line between 15 and 17 degrees is distinct. These hysteresis are caused by the flow not reattaching to the wing at the same angle it detached. Knowing when hysteresis can be created and how severe they are is very important for pilots, especially in situations where they are close to the ground, since knowing what angles of attack won't cause hysteresis can lead to better decisions and safer flights.

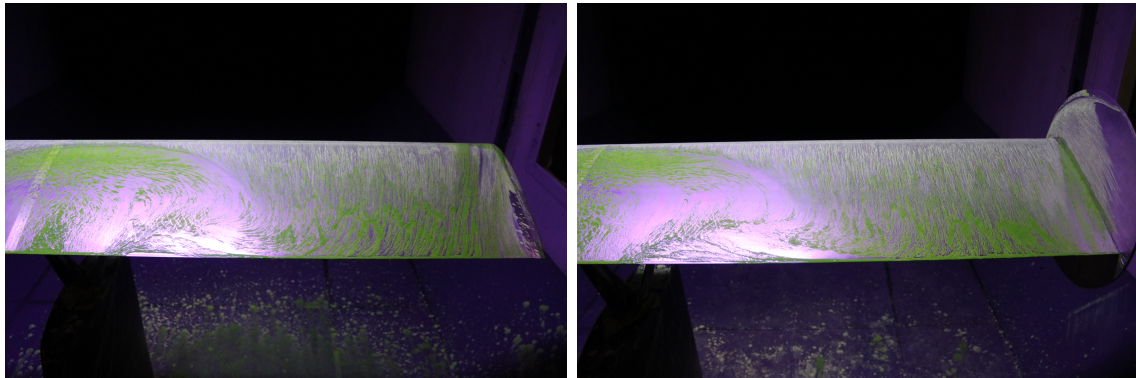


Fig. 5: China clay flow visualization on wing without end caps.

Fig. 6: China clay flow visualization on wing with end caps.

III. Conclusions

This investigation compares how characteristics such as lift, drag, and pitching moments change when disks are added to the ends of a finite wing, when evaluated at two different Reynold's numbers. With the circular endcaps installed, the wing had a slightly

steeper stall angle than the wing without endcaps. However, this difference falls within the range of uncertainty and cannot be considered a result of the installation of the endcaps. It was observed using flow visualization at the stall angle and analyzing the drag forces, that the endcaps minimized flow from the bottom of the wing mixing with flow from the top and reduced wingtip vortices that cause induced drag, lowering the drag coefficient at all angles of attack. The lift slope of the wing was unchanged by the addition of the endcaps, however, the stall angle was increased with the endcaps on. This shows that the endcaps reduced flow separation at angles of attack close to stall. With the end caps on, the moment coefficient increased at all angles of attack. These results are important to the aviation community because they show that by making slight changes to the geometry of a wing, the performance characteristics improve. This means that for a relatively low cost, manufacturers can update existing structures to improve efficiency without entirely redesigning a wing.

IV. Appendix

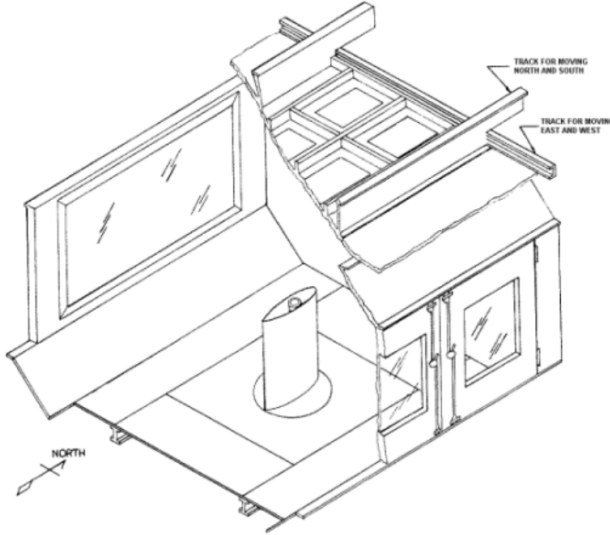


Fig. 7: KWT Cutaway